CrossMark

CASE STUDY

The Euripus tidal stream at Halkida/Greece: a practical, inexpensive approach in assessing the hydrokinetic renewable energy from field measurements in a tidal channel

Harilaos Kontoyiannis[1] · Michalis Panagiotopoulos[2] · Takvor Soukissian[1]

Abstract In the Euripus channel, we assess the hydrokinetic tidal resource at the narrowest constriction which is in the city of Halkida at the Old Bridge. This is accomplished by combining data from (a) several ADCP (Acoustic Doppler Current Profiler) cross-channel snapshot transects at the Old Bridge and (b) a 2-month current meter record obtained at 1.5 m off the bottom at the edge of the cross section at the New Bridge, which is a ∼fourfold wider constriction with lower tidal velocities compared to the Old Bridge. A linear relationship exists between the along-channel velocity at the current meter site and the maximum of the along-channel velocity on the cross section at the Old Bridge. We can, therefore, determine the cross-channel distributions of the along-channel velocity at the Old Bridge during the 2-month period of the current meter record. We examine the use of a 4-m-diameter turbine, suitable to the space limitations at the Old Bridge. This turbine functions for flow velocity values higher than ∼50 cm/s and with a nearly constant efficiency of ∼40–45 % for flow velocity higher than 50 cm/s; a constant 45 % is achieved for all velocity values higher than 150 cm/s. This machine yields an annual energy of ∼28.6 MWh, out of an existing ∼71.5 MWh for its aperture when there is zero efficiency loss. This amount of energy is not enough for wide-scale applications but it covers the needs of an exhibition place for tourists visiting Halkida, which was the first question posed in the beginning of this project.

✉ Harilaos Kontoyiannis
   hk@hcmr.gr

   Michalis Panagiotopoulos
   mpanag@cres.gr

[1] Institute of Oceanography, Hellenic Center for Marine Research, Anavyssos, Greece

[2] Center for Renewable Energy Resources, Pikermi, Greece

1 Introduction

Halkida (or Halkis or Chalkis) is the capital of the island of Evia (or Euboea or Evvoia) in Greece. Evia approaches the Greek mainland through a narrow and shallow water passage, the Euripus Strait, in the area of Halkida (Fig. 1). The city of Halkida is in fact built on both land sides of the Euripus Strait, which has its minimum width (∼45 m) and depth (∼8 m) in the city of Halkida at the location of the Old Bridge. The intense Euripus flow occurring in alternating directions is very impressive for the Greek and all the Mediterranean people who, in general, cannot readily observe strong sea water flows near their coastal cities.

Ancient Greeks were the first who attempted to study the Euripus tidal phenomenon. Aristotle's mother was from Halkida and himself spent the last part of his life in this city trying to understand the variability of the currents of Euripus. In 1981, Walter Munk visited Halkida and observed the tides to form a direct opinion of the oceanographic problem that Aristotle tried to solve (Gill 1984). In the last 100 years, there have been descriptions of the Euripus tides either in reports based on gross observations (Aiginitis 1929) or in scientific articles (Vlahakis and Tsimplis 1993; Tsimplis 1997) dealing with the sea level variability in Halkida. To our knowledge, no information based on direct current measurements at the Euripus Strait is presented in the international scientific or engineering literature.

The advantages of the hydrokinetic ocean energy in comparison to other resources of renewable energy are widespread on the world wide web in numerous articles and

Fig. 1 *Upper panels* show the location of the study area (Euripus Strait) within the Eastern Mediterranean. *Lower panel* shows an expanded view of the Euripus Strait between mainland Greece and the island of Evia. Numbers 1, 2, and 3 along with the *short* and *bold lines* show the position of the cross-channel sections at the New Bridge, the Old Bridge and the north lights, respectively. The *dashed lines* with the *arrows* show the main paths of the tidal stream
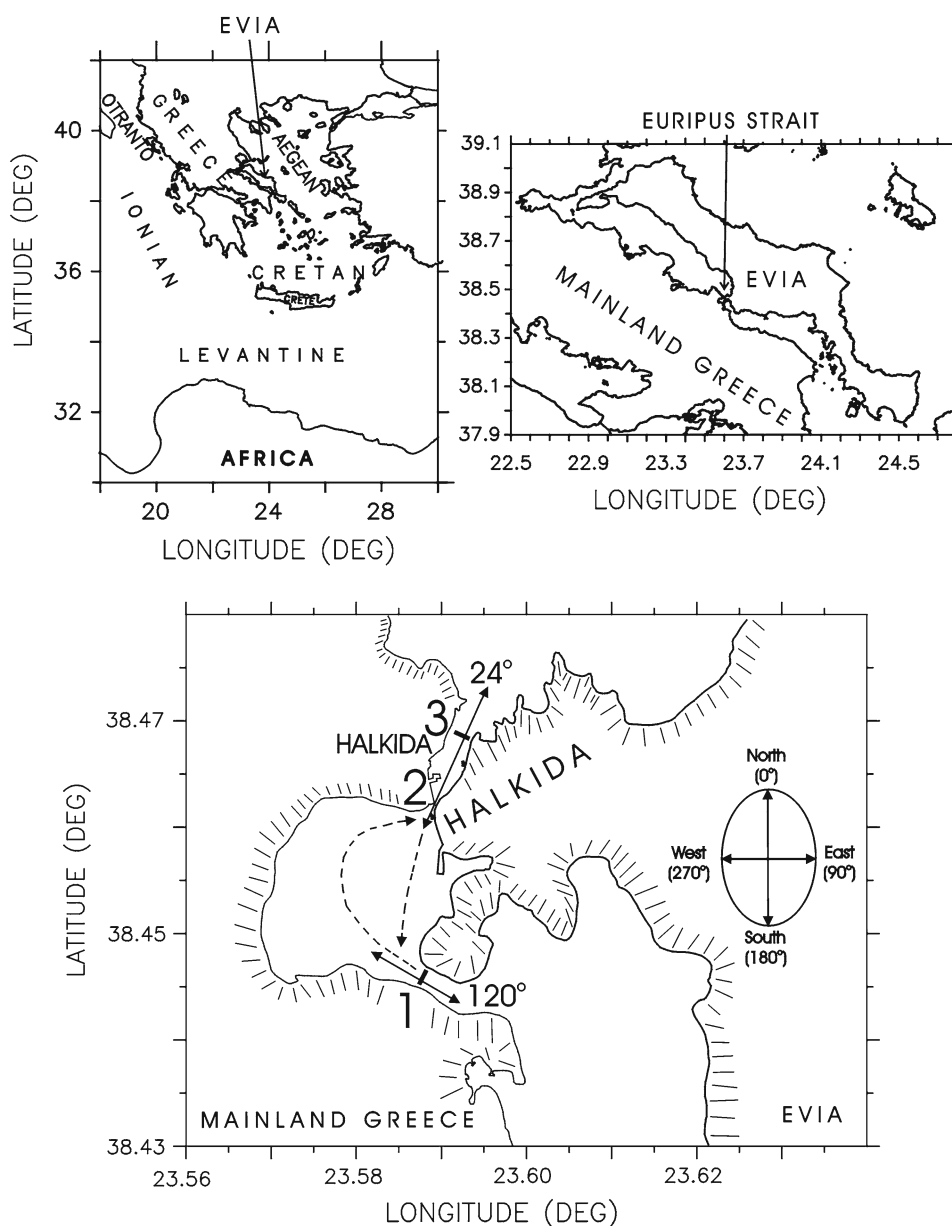
reports (http://www.inhabitat.com/2007/12/10/underwater-power-generating-ocean-turbines/). In brief, we mention that the kinetic resource available in air or water is directly related to the density of the medium and the cube of the flow speed. Given that the water density is larger than the air density by a factor of ∼800 and assuming that the kinetic energy is usually converted to electricity by a propeller-type machinery called turbine, it follows that a typical tidal flow speed of 2 m/s is nearly energetically equivalent, per propeller-unit-area, to an extreme wind speed of 19 m/s. In other words, the tidal hydrokinetic resource has a greater power density compared to wind. In addition, the hydrokinetic tidal energy is fully predictable, compared to wind, sun or wave energy and has minimal optical and noise impact.

The task in the present study is to assess the hydrokinetic power resource of the Euripus stream, where flows are very strong but tidal range is on the order of 1 m. The priority, therefore, is to quantify the current structure and variability in the stream for at least one tidal month, rather than to investigate issues pertaining exclusively to the local tides. The tidal energy assessment is carried out through direct current measurements with minimal required instrumentation, while a method is exhibited that simplifies the technical aspects of the field work. To our knowledge, the most common approach in the hydrokinetic tidal assessment appearing in the literature is through numerical modeling; examples appear in Brooks (2006, 2011), Shapiro (2011) and Adcock et al. (2013). The ultimate practical interest in the specific project was to exam-

ine if the extracted electric energy could be enough to power at least an exhibition place where the authorities of Halkida would present the history of the city to tourists and any visitors.

2 Field work and data

The field measurements were initially targeted on three cross-channel sections at along-channel points where the Euripus Strait has minimal width. Figure 1 shows the location of these sections which are (a) near the New Bridge, south of Halkida, (section width ~160 m, section depth ~8 m) (b) just under the Old Bridge within the city (section width ~45 m, section depth ~8 m) and (c) in the northern part of the Strait, between the two moored north lights, i.e., the green on the Greek-mainland side and the red on the side of Evia (section width ~200 m; ~100 m between the lights, section depth ~ 8–10 m). Based on the geomorphologic characteristics of the three sections and the flow continuity, it is expected that the kinetic resource available per unit cross-sectional area is higher by a factor of ~45–125 at the Old Bridge in comparison to the other two sections; at the Old Bridge, the cross-sectional area is lower by a factor of ~3.6–5, a typical speed is higher by the same factor, and the kinetic resource, i.e., the cubed speed, is higher by a factor of ~45–125.

The goal for any of the three sections would be to obtain the distributions of the along-channel velocity on a cross-channel transect in a continuous time series representation during a period of at least one lunar (tidal) month. A standard observational approach to achieve the specific goal would have been to deploy several current meter profilers that would sit across the bottom of the channel at each transect and continuously record the flow above them. This standard approach, however, implies several risks for instrument loss or damage and practical difficulties when having to deploy several firm structures which would host the instruments in swift currents. Following the standard approach was not feasible in our case, primarily because of financial reasons. The available instrumentation was one Aanderaa acoustic current meter (RCM9) providing point current measurements and a portable 300 kHz ADCP (Acoustic Doppler Current Profiler) made by RDI that could provide snapshot velocity profiles and transects by pinging downwards from the sea surface when it was deployed by the side of a boat at specific cross-channel locations where the boat was anchored.

We expect that the along-channel velocity values at the different along-channel locations would be interrelated. We, therefore, had to combine current meter time series, providing the time dependence at a given location, with the snapshot ADCP-transect data at a section, that provide information on the cross-channel structure of the flow, to infer the cross-channel distribution of the along-channel velocity in a

continuous time series representation for at least one lunar month. Despite that the main focus was at the Old Bridge which is the area with the highest density of kinetic available resource, we initially conducted ADCP transects on May 17, May 18 and July 7 of 2010 at all three sections each day. On the full-moon day of September 23rd 2010, we conducted five additional ADCP transects at the Old Bridge. The measurements on each ADCP section were completed in about 15–20 min. A practical difficulty concerned the deployment of the RCM9 in an area of swift currents, heavy traffic and a lot of fishing by amateurs using fishing lines. The current meter was finally deployed at the Greek-mainland edge of the section at the New Bridge, ~1.2 m off the bottom, firmly attached on a frame that sat on the bottom at a depth of 6 m. A moored red light was near the deployment position and served to easily locate the current meter during recovery in very turbid water. The current meter record covered the period from May 17, 2010 to July 15, 2010, i.e., approximately two lunar months, with half-hourly velocity and temperature measurements.

3 Results

3.1 The stream flow

Figure 2 shows the current meter flow and temperature measurements at the mainland edge of the section at the New Bridge. The record spans a total period of two lunar months. Three distinct tidal cycles between moon quarters are recorded. At a first glance, semidiurnal tides dominate the channel flow. The along-channel velocity, which is positive/negative in the direction of 300°/120°, ranges from ~ +60 to ~ −70 cm/s. The little asymmetry is likely to be mostly due to the morphology of the coastline and the resulting difference in the flow paths of the tidal stream in the area between the New Bridge and the Old Bridge (Fig. 1). These flow paths were visually observed during the field work. During the northward progression of the flow, the tidal stream is not directed directly to the Old Bridge after it exits from the New Bridge constriction but it continues along the direction of 300°, because of its inertia, and eventually flows along a longer and curved path. In this way it fills a larger portion of the basin between the New Bridge and the Old Bridge. As a consequence it is characterized by slightly lower velocities during the northward flow.

The structure of the along-channel velocity component of the Stream in the three cross sections during May 17, May 18 and July 7 is shown in Fig. 3, along with the corresponding part of the along-channel velocity recorded by the current meter. A typical jet structure with a high-velocity core is observed in most panels. At the Old Bridge and during the flow maxima of the semidiurnal cycle, high velocity values fill nearly the entire section (panels b, c).

Fig. 2 Current meter velocity and temperature measurements at the New Bridge (Fig. 1) during the period from May to July, 2010. Positive along-channel velocity is in the direction of 300°
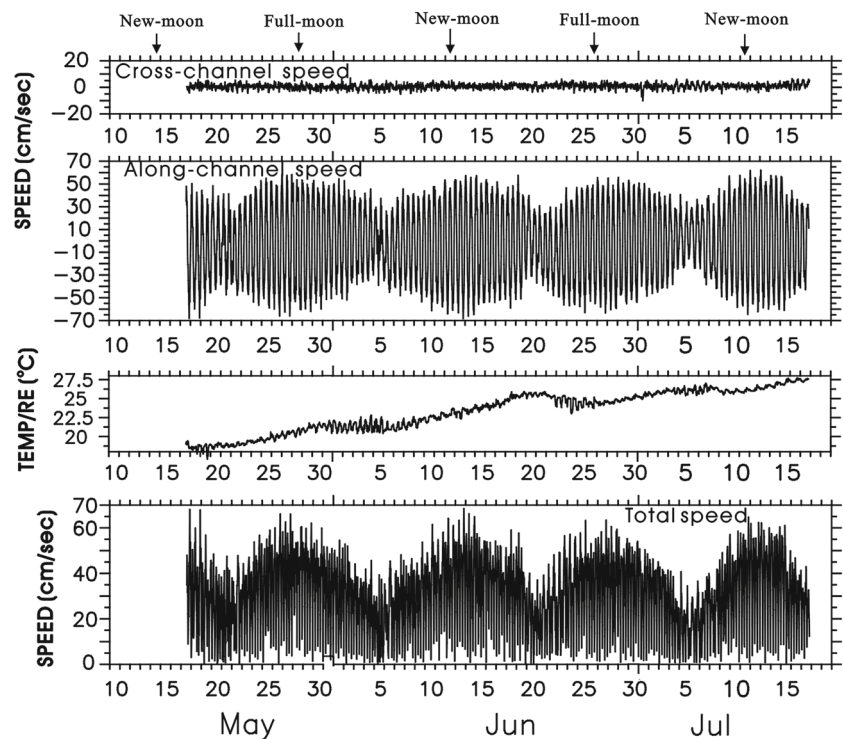

In all sections at the north lights, the highest velocity values occur at the edge on the side of Evia (panels g, h, i). This is likely to be due to the coastal morphology and the flow path followed when the Stream enters the Euripus Strait from the north–northeast. The along-channel velocity values at the Old Bridge are indeed higher than the corresponding values at the other two sections. Velocity values higher than 50 cm/s (∼1 knot) occur at the Old Bridge even at the near-bottom layers at the two edges of the cross section, where a hydro-turbine would most preferably be installed. Our attention is focused on the specific section. Figure 4 shows five additional snapshot transects at the Old Bridge on the full-moon day of September 23. The strongest along-channel flow at 24°N (Fig. 1), with velocity maxima ∼270 cm/s, occurs around 12:30 (Fig. 4b).

We seek to determine an observational/empirical quantitative relation between the along-channel current meter velocity at the New Bridge and the along-channel velocity values in the cross-channel transect at the Old Bridge. This goal is accomplished in two steps. First, it turns out that the along-channel velocity at the location of the moored current meter is linearly related to the maximum along-channel velocity in the core of the stream at the Old Bridge section shown by the inset rectangles in Fig. 3a, b, c. Second, the eight realizations (Figs. 3 and 4) of the cross-channel structure of the along-channel velocity at the Old Bridge form the basis for us to construct typical representations (structures) of the relation between the maximum along-channel velocity

in the core of the stream and the along-channel velocity in the rest of the section.

Figure 5 shows the resulting linear relationship between the along-channel current meter velocity and the maximum along-channel velocity at the Old Bridge. The open circles refer to the data of Fig. 3a, b, c with the additional point of (0, 0), which is added for reference, while the solid circles refer to the data of the full-moon ADCP transects of September 23 shown in Fig. 4a–d. As already mentioned above, Fig.4b shows the maximum positive velocity of all five panels. On September 23, there were no direct current meter measurements; the corresponding current meter values on September 23 were determined as follows: in the previous full-moon flows, that occurred on May 28 and June 26 (Fig. 2), the along-channel current meter velocity values were very nearly the same. Figure 6 shows their average and their standard deviation; both quantities are time-referenced with respect to the 'zero hour' of the highest positive velocity, i.e., towards 300°N (Fig. 1). The information on Fig. 6 is used to estimate the corresponding current meter measurements that would have been recorded around the peak positive flow at the Old Bridge on the full-moon day of September 23. The information in Fig. 4e is not used because at the corresponding time lag, relative to the peak flow, the uncertainty of the averaged current meter velocity, indicated by the standard deviation, is very high (∼ ±20 cm/s). The resulting linear relationship between the maximum along-channel velocity at the Old Bridge (V_{max}) and the along-channel velocity at the position of the current meter (V_{cm}) is
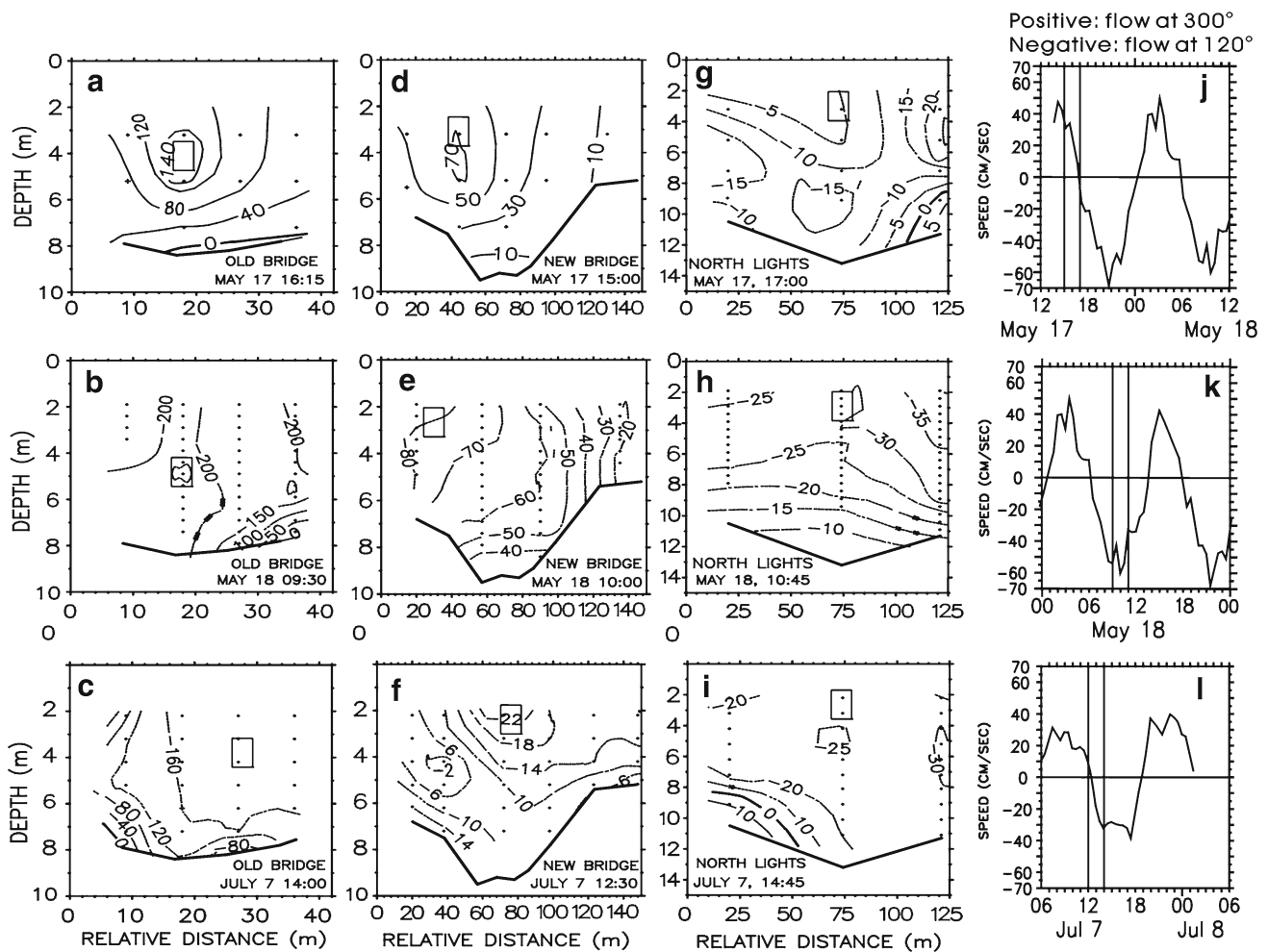
Fig. 3 Panels **a–i** snapshot distributions of along-channel current velocity that is normal to the cross-channel sections at the Old Bridge, New Bridge and the north lights in the ADCP surveys during date and time as indicated in the lower part of each panel. In all panels, mainland Greece is on the *left side* and Evia is on the *right side*. The *rectangle in each panel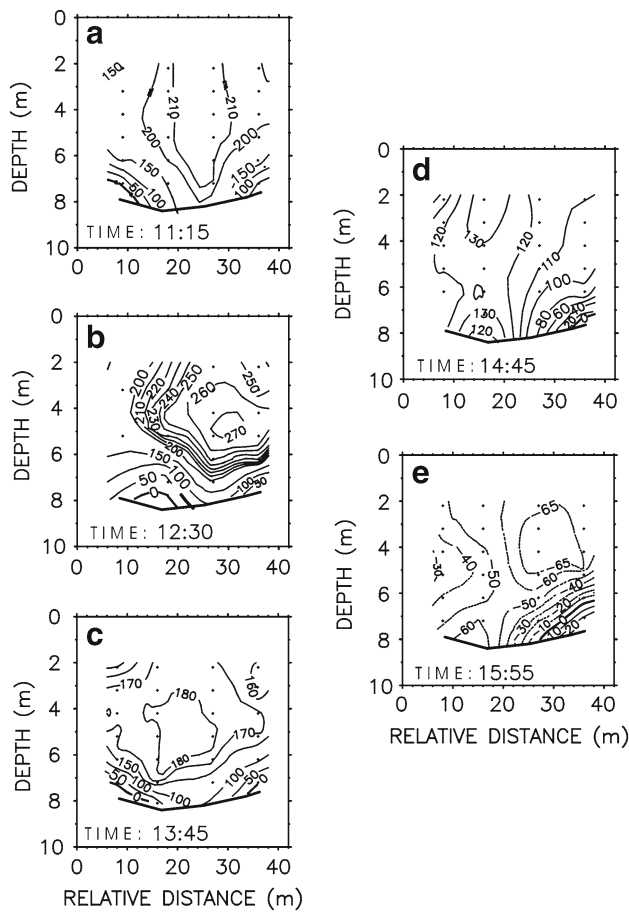* shows the location and the approximate value of the maxi-mum along-channel velocity. *Small crosses* indicate positions of ADCP data. Panels **j–l** Time series of current meter velocity normal to the New Bridge cross section during the ADCP surveys. *Vertical lines* indicate the time interval for the completion of the three ADCP transects within a specific day. The time axes show days and hours of local time

$$V_{\max} = 4.58 \, V_{cm} - 3.92, \tag{1}$$

with a correlation coefficient ~ 0.97.

We then seek a relationship or equivalently a structure that could generate the approximate along-channel flow velocity values on the entire Old Bridge cross section at a given time if the section-maximum along-channel velocity is provided. This points towards dividing the along-channel velocity values on each transect at the Old Bridge by their maximum value for the given transect. The eight available cross-channel transects at the Old Bridge (Figs. 3 and 4) are listed in Table 1 along with the corresponding section-maximum and current meter velocity values. The resulting normalized (non-dimensional) structures for each transect can then be appropriately averaged to produce a representative mean nor-malized structure for the entire range of tidal velocity values. Prior to that, however, we allow for a cross-section struc-ture dependence of the section-maximum velocity, and we use four different normalized structures of cross-channel dis-tributions depending on the value of the section-maximum along-channel velocity or equivalently on the value of the along-channel current meter velocity. The V_{cm} values range from ~ -70 to $+60$ cm/s (Figs. 2, 6). For V_{cm} ($V_{\max}$) veloc-ity values greater than $+40$ ($+180$) cm/s and lower than -40 (-187) cm/s we used, correspondingly, the so-called 'higher positive' and 'higher negative' normalized structures (Fig. 7a and c) which are given by the mean of the structures in Fig. 4a, b for the 'higher positive' and the structure in Fig. 3b for the 'higher negative'. For V_{cm} velocity values in between them ($40 > V_{cm} > 0 > V_{cm} > -40$) we used the 'lower

Fig. 4 Snapshot distributions of current velocity normal to the cross-channel sections at the Old Bridge during the five ADCP transects in September 23, 2010. The *labels* in the *lower part* of *each panel* show the approximate time when half of the respective transect was completed. Each transect lasted approximately ~15–20 min. *Small crosses* indicate positions of ADCP data
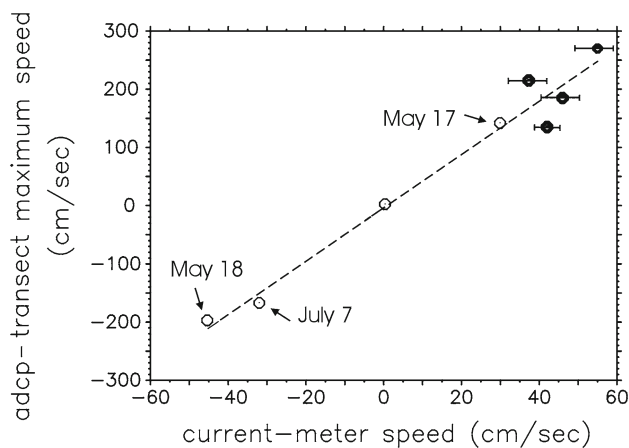
Fig. 5 Relationship between along-channel velocity at the current meter position in the New Bridge area and the maximum along-channel velocity in the ADCP transects at the Old Bridge

positive' and 'lower negative' normalized structures (Fig. 7b and d) which were given by the mean of the structures in Figs. 3a and 4c, d and for the 'lower positive' and the mean of the structures in Figs. 3c and 4e for the 'lower negative'. The overall mean normalized velocity structure at the Old Bridge, i.e., the mean of the structures in Fig. 7a–d is shown in Fig. 7e. The threshold value of ± 40 cm/s is a first choice for differentiating between higher positive and higher negative structures. Our results on extractable power density (power per unit cross-sectional area) are not strongly dependent on this particular choice. A threshold value of ± 30 cm/s results in ~12 % differences, with respect to the case of ± 40 cm/s, in mean power densities at particular subsections of the entire cross section, whereas the mean power density over the entire cross section is affected by less than 5 %. These subsections are shown in the next section in the discussion with respect to Fig. 9. In addition, we show that the computations which do not consider a dependence of the along-velocity distribution on the section-maximum velocity and use the overall mean structure (Fig. 7e) result in comparable estimates in power densities with the computations that use the structures of Fig. 7a–d.

3.2 The hydrokinetic energy

In the theoretical case of a stream flow with no energy-converting machinery in it, the horizontal kinetic energy flux E, i.e., the energy that is transferred in time Δt through an area ΔS perpendicular to the flow is given by $E = 1/2 \ \rho \ V^3 \Delta S \Delta t$, where ρ is the fluid density and V the fluid velocity perpendicular to ΔS. In the presence of one and only ideal turbine with 100 % efficiency in a channel with a cross-sectional area much larger than that of the turbine, the kinetic energy transferred through a unit cross-sectional area of the turbine, i.e., the available kinetic energy density, is reduced by the Lanchester–Betz factor (16/27) relative to the upstream kinetic energy flux per unit cross-sectional area, because of the pressure drop and the work done by the fluid as it crosses the cross-sectional area of the turbine (Lanchester 1915; Bergey 1980). The available power density (APD) is, therefore, given by

$$\text{APD} = 8/27 \rho V^3 \qquad (2)$$

Garret and Cummins (2005, 2007, 2008) have examined the influence of combinations of idealized (100 % efficiency) turbines, called fences, on the maximum extractable power ($P_{\max}$). In brief, $P_{\max} = (8/27) \ (1-\varepsilon)^{-2} \ \rho \ A \ V^3$, where $\varepsilon = A/\text{Ac}$ is the fractional area of the channel occupied by the turbines. For a single turbine ($\varepsilon \ll 1$) the amplification factor $(1-\varepsilon)^{-2}$ is negligible and the maximum power is given by the Lanchester–Betz limit [(8/27) ρ A V^3]. In any realistic case, the turbine(s) efficiency has to be

Table 1 Figures with available realizations of cross-section distributions of along-channel velocity at the Old Bridge along with the section-maximum velocity and the corresponding current meter velocity through the linear relationship of Fig. 5

| Figure:	Fig. 3b	Fig. 3c	Fig. 4e	Fig. 4d	Fig. 3a	Fig. 4c	Fig. 4a	Fig. 4b
Maximum velocity at Old Bridge section (cm/s)	−200	−160	−65	+130	+140	+180	+210	+270
Current meter velocity (cm/s)	−43	−34	−13	+28	+30	+40	+47	+60
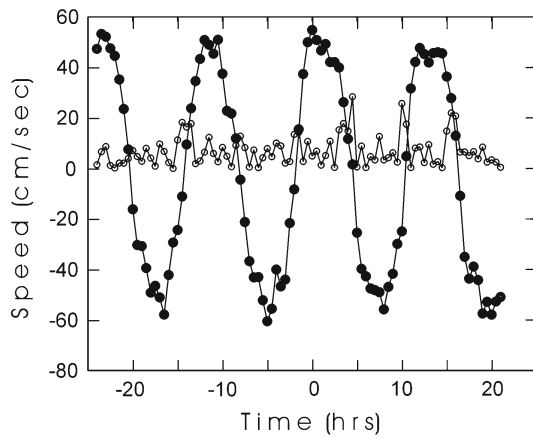
Fig. 6 Mean (*solid circles*) and standard deviation (*open circles*) of the along-channel current meter velocity during the full-moon days of May 28 and June 26. Time axis is in hours relative to the time of the occurrence of the highest positive velocity, i.e., at 300°N (Fig. 1)

considered along with the influence on the flow of the structure(s) supporting the turbine(s). In our case we first carry out calculations of APD based on the Lanchester–Betz limit and then we consider the additional loss of a hypothetical turbine with specific efficiency based on available turbine technology in 2010.

Figure 8a shows the timeseries of the section-mean APD at the Old Bridge during the period of the current meter measurements. In this calculation, we used the four different velocity structures, shown in Fig. 7, that depend on the section-maximum velocity. Positive and negative values of APD correspond to occasions when flow is in the direction of 24° and 204°, respectively. The time series of the section-mean APD apparently exhibits tidal variability with much stronger absolute peaks during the southwestward (204°) flows. The positive and negative maxima of APD are near ∼4 and ∼7 kW/m², respectively. Figure 8b is a histogram showing the distribution as a percent of occurrence of the absolute values of the APD. For nearly 62 % of the time in the 2-month deployment period the section-mean APD is higher than ∼0.5 kW/m², whereas for nearly 36 % of the time it is higher than 1.5 kW/m². The section-mean APD is ∼0.9 kW/m².

Apart from the information that concerns the section-mean APD at the Old Bridge, the existing APD in the different parts of the Old Bridge section is of practical importance. Figure 9
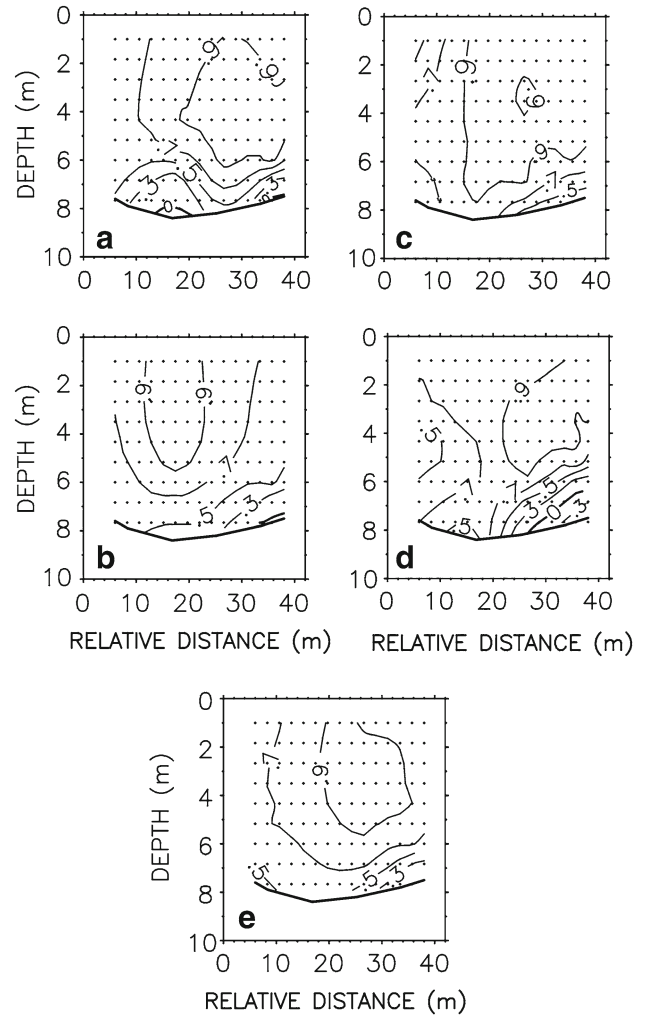

Fig. 7 Panels **a–d** Normalized distributions of along-channel velocity relative to the maximum along-channel velocity V_{max} at the Old Bridge cross-channel transect for $V_{max} > 180$ cm/s (panel **a**; higher positive), $0 < V_{max} < 180$ cm/s (panel **b**; lower positive), $V_{max} < −187$ cm/s (panel **c**; higher negative) and $−187 < V_{max} < 0$ cm/s (panel **d**; lower negative). Panel **e** Overall mean normalized along-channel velocity distribution constructed as average of distributions in panels **a–d**. *Small crosses* indicate the grid of the interpolated along-channel velocity values

shows the mean of the absolute APD values at the six different subsections in which we divide the entire Old Bridge section. These values range from ∼0.65 kW/m² in subsections S1 and S6 to ∼1.13 and 1.16 kW/m² in subsections S3 and S5, respectively.

Fig. 10 A hypothetical hydroturbine machine efficiency as a function of flow velocity
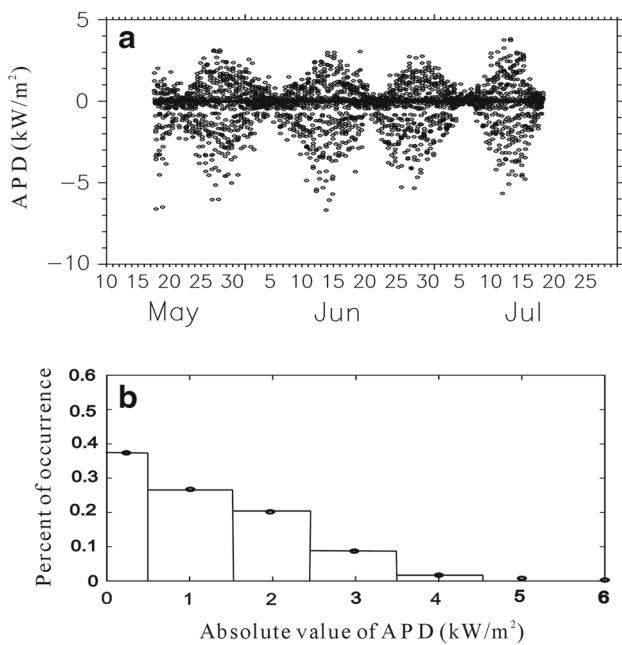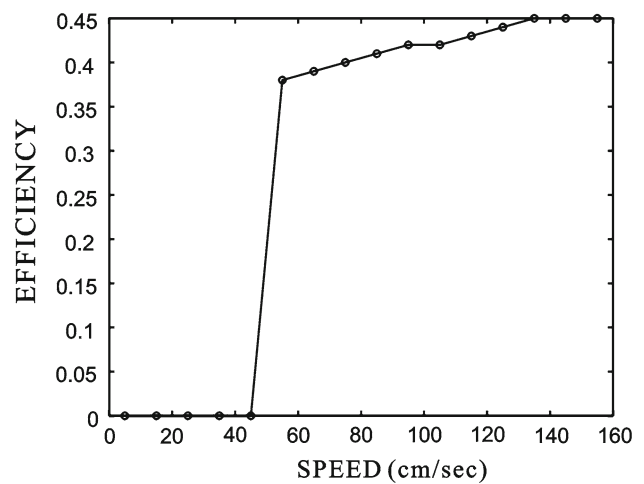
Fig. 8 *Upper panel* time series of section-mean Available Power Density (APD $= (8/27)\rho V^3$) for the entire cross-channel section at the Old Bridge from May to July, 2010. Positive (negative) values are for flow to 24° (204°). *Lower panel* Histogram (percent of occurrence) distribution of the absolute values of the APD that appears in the *upper panel*
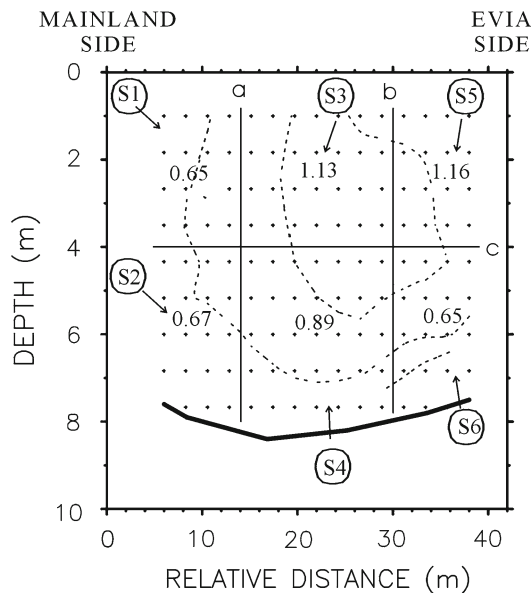
Fig. 9 Mean Available Power Density (APD) values in kW/m² for the period May to July, 2010 (Fig. 8, *upper panel*) indicated by the *arrows* for the subsections S1–S6 in which the entire Old Bridge cross-channel section is divided by *lines* **a**–**c**. *Dashed lines* show the overall mean normalized along-channel velocity distribution of Fig. 7e. *Small crosses* indicate the grid of the interpolated along-channel velocity values

In the restricted area of the Old Bridge, it would be suitable to install a horizontal-axis turbine with a rotor diameter around 4–6 m which will operate at flow velocity val-

ues between 0.5 and 2.5 m/s. We, therefore, examine the power density provided by a machine with the efficiency shown in Fig. 10, which operates for this velocity range and is taken from the report 'Assessment of Tidal Energy Resources' of the European Marine Energy Centre Assessment of Tidal Energy Resources (2009) (http://www.emec.org.uk/assessment-of-tidal-energy-resource). These specifications imply that the machine (a) does not work when the flow velocity is less than 50 cm/s, (b) reaches its maximum efficiency, which is 45 %, near a flow velocity of ∼150 cm/s and (c) does not exceed this efficiency limit when the flow velocity is higher than ∼150 cm/s. The so-called 'rated velocity', for which the efficiency levels-off to its maximum value, is 150 cm/s for this hypothetical turbine. The particular specifications, however, represent a typical case of a hydroturbine with a rotor of 20 m diameter. A question that arises is 'how much the specific efficiency of 40–45 % can differ for a machine with a 4–6 m diameter?' Simulations for conceptual optimal rotors in stall-regulated hydrokinetic turbines with a diameter of 5 m, have shown that the maxima in the optimal efficiencies could be as high as 48 % (Sale et al. 2009). Based on this evidence, we expect that using an efficiency of 40–45 %, as in Fig. 10, is still realistic and does not affect the final conclusions on the very weak extractable energy. On the other hand, the emphasis in this work is mostly on the method followed in the field campaign to determine the time dependence and the cross-sectional structure of the tidal flow via direct field measurements.

In what follows, the power density (PD) output will imply the available power density for one machine, as specified in Eq. (2), which, in addition, will be subjected to the efficiency restrictions of Fig. 10. Table 2 lists the power density (PD) output in terms of mean, standard deviation and maximum value of PD in each of the six sub-sectional areas that com-

Table 2 Basic statistics of the Power Density (PD) output for the machine efficiency shown in Fig. 10 at the Old Bridge entire section (S_{all}) and parts of it [subsections S1 through S6 (Fig. 9)] during the period from May 17 to July 15, 2010 (Fig. 8)

Area	Mean PD (APD) (kW/m^2)	Ratio of mean values	Standard deviation of PD (APD) (kW/m^2)	Ratio of standard deviation values	Maximum PD (APD) (kW/m^2)	Ratio of maximal values
S1	0.28 (0.65)	0.43	0.35 (0.78)	0.45	2.3 (5.2)	0.44
S2	0.27 (0.67)	0.40	0.43 (0.95)	0.45	2.8 (6.3)	0.44
S3	0.50 (1.13)	0.44	0.55 (1.22)	0.45	3.4 (7.6)	0.45
S4	0.38 (0.89	0.43	0.47 (1.05)	0.45	3.1 (6.8)	0.45
S5	0.48 (1.16)	0.41	0.59 (1.29)	0.46	3.7 (8.2)	0.45
S6	0.26 (0.65)	0.40	0.34 (0.74)	0.46	1.9 (4.3)	0.45
S_{all}	0.38 (0.91)	0.42	0.47 (1.03)	0.46	3.0 (6.7)	0.45
S_{all}^{*}	0.42 (0.96)	0.44	0.46 (1.02)	0.46	2.9 (6.4)	0.45

Numbers within parentheses are area-specific APD statistics for an ideal machine (Eq. 2). PD output values are considered as positive for both flow directions, i.e., 24°N and 204°N. In all PD statistics, four different flow structures, depending on the maximum along-channel current velocity (Fig. 7a–d) have been considered apart from the statistics for the entire section in the last line (S_{all}^{*}), where the mean velocity structure of Fig. 7e is used. Each cell with a ratio value presents the ratio of the numbers with and without parentheses appearing in the corresponding cell immediately to the left of it S_{all}^{*}; The mean structure of Fig. 7e is used

pose the entire Old Bridge section. To ease the comparison, we list in parentheses the APD estimates of Eq. (2), i.e., the case of one ideal machine without efficiency loss. The last two lines in the table refer to the PD calculations for the entire section when we use (a) the four different flow structures depending on the maximum velocity (Fig. 7a–d) and (b) their mean (Fig. 7e). The resulting PD mean values in all subsections are in general 40–45 % of the corresponding APD values. Therefore, there is an approximate ~60–65 % loss due to machine efficiency. The higher mean PD values are in subsections S3 and S5, i.e. in the upper central part of the flow and in the upper part in the side towards the Evia. A similar percentage of reduction, in the presence of machine loss, also occurs in the maximum absolute values of PD. As was observed in Fig. 8, the instantaneous APD values are highly variable. Indeed, in all subsections and in all the respective calculations, with or without machine loss, the standard deviation values of PD exceed those of the mean. Finally, the last two lines of Table 2 show that no significant changes in the mean, standard deviation and the maximum PD for the entire Old Bridge section occur if we utilize the overall mean structure for the velocity distribution (Fig. 7e) versus the four different structures depending on the maximum section velocity (Figs. 7a–d).

In principle, the above results on the power density output are valid for the 2-month deployment period. Despite that the pure tidal motion has practically no energy in periodicities longer than a lunar month, a question that in fact remains is if these results can be extrapolated in time so as to produce estimates of the yearly output of electric energy in MWh. To try to answer this question we first have to separate the pure tidal motion from the tidal residual in the observed flows and compare them to one another. This can be routinely performed on the time series of the along-channel
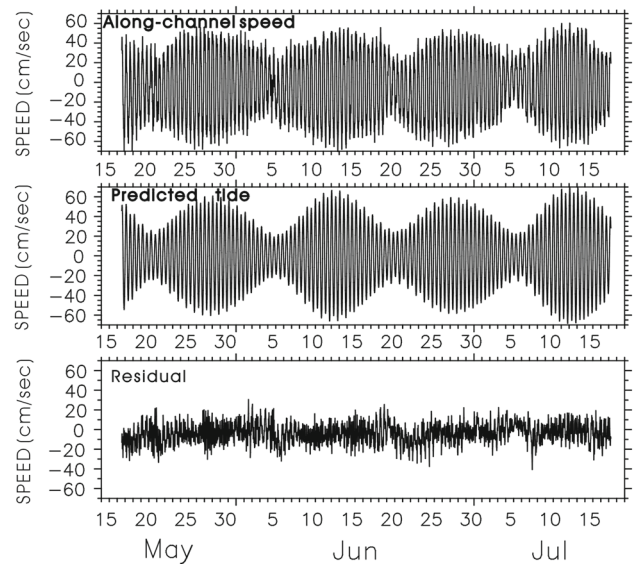
Fig. 11 The decomposition of the along-channel current meter velocity at the New Bridge (*upper panel*) into predicted tidal motion (*middle panel*) and tidal residual (*lower panel*)

velocity of the current meter data with the Tidal Response Method (Munk and Cartwright 1966; Mofjeld and Wimbush 1977). In this method the tide generating potential that originates from the known earth, moon and sun orbits is fitted in a least-squares sense on the available tidal time series at an observational point. This allows the computation of the tidal response, the predicted tide and the residual nontidal signal. There is no a priori assumption of predominant tidal frequencies in the observations, as in the harmonic tidal analysis; the importance of the various tidal constituents can be computed via the response admittance after the fit is completed. Figure 11 shows the along-channel velocity, repeated

from Fig. 2, the pure tidal motion or predicted tide and the tidal residual. The M2, S2 and MN4 (semi-daily lunar and solar plus the shallow water quarter-diurnal) are the dominant constituents of the predicted tide which has a mean magnitude of ~28 cm/s, for both positive and negative velocity values, i.e, flow towards 300° and towards 120°, respectively (Fig. 1). The residual flow is much weaker with a mean magnitude of positive velocity values approximately ~6.5 cm/s and a mean magnitude of negative velocity values approximately ~9.5 cm/s. The existing asymmetry of the along-channel velocity, discussed earlier, is in fact contained in the residual flow which has an overall mean of −3.9 cm/s, i.e., mean flow towards 120°. These results show that the pure tidal motion at the New Bridge has a velocity magnitude larger than the velocity magnitude of the residual flow by a factor of ~3–4. The resulting APD due to the pure tidal motion will, therefore, be higher than the APD of the residual flow by a factor of ~50. We cannot determine the pure tidal motion and the tidal residual at the Old Bridge with direct in situ measurements. However, using the linear relationship between the current meter along-channel velocity and the maximum along-channel velocity of the cross section at the Old Bridge and considering that the tidal component of the maximum along-channel velocity has zero mean, unlike its residual component, it is plausible to assume that

$$V_{\text{max\_tid}} = 4.58\, V_{\text{cm\_tid}} \qquad (3)$$

and

$$V_{\text{max\_res}} = 4.58 V_{\text{cm\_res}} - 3.92 \qquad (4)$$

where $V_{\text{max\_tid}}$, $V_{\text{max\_res}}$ are the tidal and the residual components of the maximum along-channel velocity at the Old Bridge and $V_{\text{cm\_tid}}$, $V_{\text{cm\_res}}$ are the tidal and the residual components of the along-channel current meter velocity. Therefore, it is obvious that the gross results of magnitude comparison between the pure tidal motion and the tidal residual at the New Bridge are not altered significantly at the Old Bridge. The APD due to the residual flow at the Old Bridge is again less than the APD due to the pure tidal flow by nearly a factor of ~50. The least amount of annual tidal energy is expected to originate from the subsection S6 (Table 2). Therefore, a 2-month mean PD of ~0.26 (APD ~0.65) kW/m^2 in area S6 is expected to result in approximately ~28,600 (71,500) kWh within a year if we use a hydro-turbine with a radius of 2 m and an efficiency shown in Fig. 10; numbers in parentheses assume no loss due to turbine efficiency.

4 Summary and conclusions

The basic advantage of the tidal hydrokinetic resource in comparison to other forms of green energy is that it is reliably predictable. On the other hand, the areas where this energy can be harvested are usually coastal channel constrictions with increased sea traffic for commercial or recreational purposes so as to hinder the direct current measurements in the beginning of a green energy project and the harvesting installations later on.

In this work, we estimate the kinetic power resource of the Euripus tidal stream in the city of Halkida in Greece using direct current measurements. This is accomplished through an inexpensive non-standard procedure that eases the tasks of the field work and minimizes the risks for instrument loss or damage. We take advantage of the existing relationship of the along-channel velocity at the various locations along the channel. Therefore, we combine time series of current point measurements at a location where instrument deployment is fairly easy and non-risky, with snapshot shipboard ADCP cross-channel transects at the location with minimal width and highest along-channel velocity values, where the kinetic resource per unit cross-sectional area is maximal. This allows us to quantitatively infer the full cross-sectional structure and variability of the along-channel flow at the location with the highest velocity values without having to deploy a cross-channel array of velocity profilers in that location.

The constriction at the Old Bridge, with a width of ~45 m and a depth of ~8 m, has APD values that are higher by ~2 orders of magnitude than the APD values at the other two locations that we considered along the channel. The 2-month average APD values of the cross section at the Old Bridge vary spatially within the cross section from ~1.16 kW/m^2, in the upper four meters of the section-edge near Evia, to ~0.65 kW/m^2, in the deeper four meters of the section, while the section-mean instantaneous APD values on full-moon and new-moon days can be as high as ~7 kW/m^2, assuming no loss due to hydro-turbine efficiency. For a hydro-turbine which functions only for flow velocity greater than ~50 cm/s and with a nearly constant efficiency of ~40–45 % for all velocity values higher than 50 cm/s, the corresponding 2-month average PD values at the Old Bridge vary from 0.50 kW/m^2, in the upper 4 m, to 0.26 kW/m^2 in the deeper four meters of the section.

Due to the space-restriction at the Old Bridge constriction, only small-size turbines with maximum diameter of ~4 m can be used to extract the energy. Such a turbine that would function in the deeper four meters of the section-edge near Evia, i.e., in area S6 in Table 2, with PD of 0.26 kW/m^2 (APD ~0.65 kW/m^2), would yield ~28.6 MWh annually, out of an existing ~71.5 MWh for its aperture when there is no conversion loss. The fraction of the converted energy is ~28.6/71.5 MWh, i.e., ~0.4, while the degree of utilization

or capacity factor, defined as the ratio of the annual energy delivered to the electric grid to the annual output energy if the machine was operating at the rated velocity (150 cm/s in this case) for an entire year (Lalander et al. 2013), is $\sim 28.6/58.66$ MWh, i.e ~ 0.49. This machine could cover the energy needs of ~ 1.6 homes, assuming a maximum monthly demand of 1.5 MWh per home (Brooks 2011). The demands of another ~ 1.6 homes could be covered by a similar turbine positioned in the deeper four meters at the section-edge near the mainland, area S2 in Table 2, where the PD is ~ 0.27 kW/m^2 (APD ~ 0.67 kW/m^2). The energy that can be harvested is not enough to cover the needs of a small-size community, but it can certainly cover the needs of an exhibition place for tourists and visitors interested in Halkida's history through the many centuries of its existence.

The specific study area is characterized by a low hydrokinetic tidal potential with respect to other well-known areas of great general interest that are mentioned in the references of the introduction. However, this work provides a hint that the exhibited simple procedure which employs only direct current measurements is likely to be applicable to other tidal channels to the extent that the along-channel velocity values at neighboring locations along the channel are interrelated though an empirical observational relationship that will have to be determined in each case.

References

Adcock TAA, Draper S, Houlsby GT, Borthwick AGL, Serhalioglu S (2013) The available power from tidal stream turbines in the Pentland Firth. In: Proceedings of the Royal Society A 469:20130072

Aiginitis D (1929) The problem of the Tides of Euripus. In: Proceedings of the Academy of Athens A p 49059

Assessment of Tidal Energy Resources (2009) European Marine Energy Centre (EMEC) www.emec.org.uk/assessment-of-tidal-energy-resource

Bergey KH (1980) The Lanchester-Betz limit. J Energy 3:382–384

Brooks DA (2006) The tidal-stream energy resource in Passamaquoddy-Cobscook Bays: a fresh look at an old story. Renew Energy 31:2284–2295

Brooks DA (2011) The hydrokinetic power resource in a tidal estuary: the Kennebec river of the central maine coast. Renew Energy 36:1492–1501

Garret C, Cummins P (2005) The power potential of tidal currents in channels. In: Proceedings of the Royal Society A 461(2563):2572

Garret C, Cummins P (2007) The efficiency of a turbine in a tidal channel. J Fluid Mech 588(243):251

Garret C, Cummins P (2008) Limits to tidal current power. Renew Energy 33:2485–2490

Gill A (1984) Walter, Aristotle and the Tides of the Euripus. In: A celebration in Geophysics and Oceanography—1982. In Honor of Walter Munk on his 65th birthday, October 19, 1982. Scripps Institution of Oceanography Reference Series 84–5, March 1984. Library of Congress No 84–181943

Lalander EM, Grabbe ML (2013) On the velocity distribution for hydro-kinetic energy conversion from tidal currents and rivers. J RenewSustain Energy 5:023115. http://dx.doi.org/10.1063/1.4795398

Lanchester FW (1915) A contribution to the theory of propulsion and the screw propeller. Trans Inst Naval Archit LVII:98–116

Mofjeld H, Wimbush M (1977) Bottom pressure observations in the Gulf of Mexico and Caribbean Sea. Deep Sea Res 24:987–1004

Munk W, Cartwright A (1966) Tidal spectroscopy and prediction. Philos Trans Royal Soc Lond A 259:533–581

Sale D, Jonkman J, Musial W(2009) Hydrodynamic optimization method and design code for stall-regulated hydrokinetic turbine rotors. ASME 28th International Conference on Ocean offshore and Arctic Engineering, Honolulu, Hawai

Shapiro GI (2011) Effect of tidal stream power generation on the region-wide circulation in a shallow sea. Ocean Sci 7:165–174

Tsimplis M (1997) Tides and sea-level variability at the Strait of Euripus. Estuar Coast Shelf Sci 44:91–101

Vlahakis GN, Tsimplis M (1993) The Euripus problem: review and a proposal. Proceedings of the 4th National Symposium of Oceanography and Fisheries, Hellenic Centre for Marine Research. (In Greek with English abstract)